PHYSICAL REVIEW B VOLUME 50, NUMBER 5 1 AUGUST 1994-I

Investigation of precipitate formation on laser-ablated $YBa_2Cu_3O_{7-\delta}$ thin films

J. P. Gong*
Research Laboratory of Engineering Materials, Tokyo Institute of Technology, 4259 Nagatsuta, Midori-ku, Yokohama 227, Japan

M. Kawasaki†
Research Laboratory of Engineering Materials, Tokyo Institute of Technology, 4259 Nagatsuta, Midori-ku, Yokohama 227, Japan and PRESTO, Research Development Corporation of Japan, 4259 Nagatsuta, Midori-ku, Yokohama 227, Japan

K. Fujito, R. Tsuchiya, M. Yoshimoto, and H. Koinuma
Research Laboratory of Engineering Materials, Tokyo Institute of Technology, 4259 Nagatsuta, Midori-ku, Yokohama 227, Japan
(Received 15 November 1993; revised manuscript received 4 March 1994)

We have investigated systematically the particle formation on the surface of high-quality $YBa_2Cu_3O_{7-\delta}$ (YBCO) epitaxial films grown by pulsed laser deposition. Scanning-Auger-electron spectroscopy identified two types of precipitates, i.e., $BaCuO_2$ and CuO, on the films deposited from a stoichiometric YBCO target. The coexistence of these two phases with a YBCO matrix film is well explained by the pseudoternary phase diagram of $YO_{1.5}$-BaO-CuO, assuming a slight Y deficiency in the film. The precipitate formation was reduced when the films were grown under conditions slightly deviated from the optimum for the formation of well-equilibrated, highly crystalline, and high-T_c and high-J_c films. Under such thermodynamically off-equilibrated conditions, the phase separation into YBCO and secondary phases is presumed to be kinetically prevented to give solid-soluted films and off-stoichiometric compositions and inferior crystallinity and superconductivity. The film-thickness dependences of the precipitate density and size were quantitatively analyzed by scanning electron microscopy to indicate that the nucleation of precipitates occurred by the initial 50 nm growth of the film to be followed by the increase of the precipitate's size. The use of off-axis polished substrates could successfully suppress the nucleation of the precipitates. A possible mechanism of precipitate formation is proposed.

I. INTRODUCTION

High-T_c epitaxial films are abundant in various defects and surface precipitates due probably to their complexity in chemical compositions and crystal structures. From the viewpoint of electronic device application, the presence of precipitates is one of the main obstacles to the fabrication of Josephson tunnel junctions. The understanding both of the formation mechanism of precipitates and of its relationship to the crystal-growth mechanism is essential to control the thin-film growth of high-T_c oxide. Surface precipitates have been observed on $YBa_2Cu_3O_{7-\delta}$ (YBCO) films grown by virtually all vapor deposition methods, such as pulsed laser deposition (PLD),[1,2] sputtering,[3,4] and metal-organic chemical-vapor deposition.[5] Previous studies have shown that precipitate formation is very sensitive to the growth conditions and stoichiometry.[6–8] Precipitates reported so far consist of the following phases: CuO,[9,10] Y_2O_3,[4,9,11,12], $YCuO_2$,[13] $BaCu_2O_2$,[9], YCu_2O_5,[9] Y_2BaCuO_{5-x}.[9,10] The formation mechanism of such high density of surface precipitates has been phenomenologically investigated but not yet understood quantitatively.

In one of our recent papers,[14] we reported that the simultaneous observation of the atomic images and the superconducting gap spectrum could be achieved by a low-temperature scanning tunnel microscope and spectroscope on high-quality YBCO thin films with a well-equilibrated and relaxed crystal matrix grown by PLD. Scanning electron microscope (SEM) observation revealed the presence of high-density (10^7 cm^{-2}) precipitates on these film surfaces. Here we report a systematic study of the precipitate formation on the YBCO films: the variation of precipitate density accompanied by the change of the film-growth conditions and the relationship between the film crystallinity and the density of surface precipitates. Discussions are made with respect to a possible phase segregation mechanism during the heteroepitaxial crystal growth of YBCO films.

II. EXPERIMENT

YBCO thin films were deposited on $SrTiO_3$(100) substrates by ArF excimer laser ablation from a stoichiometric target which was placed 3 cm away from the substrate. Films were prepared under wide growth conditions: oxygen pressure from 100 to 400 mTorr, substrate temperature from 725 °C to 735 °C, and laser fluence from 0.58 to 1.42 J/cm^2 varied either by changing the laser power or by defocusing the incident laser beam. The best crystallinity films were obtained under conditions of 400 mTorr, 730°C, and 1.2 J/cm^2 laser fluence.[15] The deposition rate ranged from 0.05 to 0.10 nm/pulse. After the film deposition, the chamber was filled with 700-Torr oxygen and the sample was kept for 30 min at 400 °C before cooled down to room temperature. Experi-

0163-1829/94/50(5)/3280(8)/$06.00

mental details were described in a previous paper.[14]

Surface morphology of the film was examined using a high-resolution SEM. The microscopic composition of the precipitates was analyzed by scanning-Auger-electron spectroscopy (AES) operated with a beam diameter of 30 nm at an accelerating voltage of 10 kV. The total composition of the films was analyzed by inductively coupled plasma analyzer (ICP). The solution concentration for ICP analysis was about 1 ppm in 1% HCl, which resulted in the accuracy of 5% for Ba/Y and 10% for Cu/Y. The crystal structure of the film was analyzed by means of a $2\theta/\theta$ x-ray diffractometer (XRD).

III. RESULTS AND DISCUSSION

A. Origin of particles

The particles observed on the YBCO film are believed to originate from two sources. One is the droplets which directly come from the target because of the explosive laser-ablation process.[1,2,16] The other is the precipitates segregated from the YBCO matrix due either to the cationic compositional inhomogeneity or off stoichiometry.[8,9] For elucidating the origin of the particles discussed in this paper, we show, at first, the dependence of film surface morphology on the substrate orientation.

Figure 1 shows the SEM photographs of the *c*-axis-oriented (a) and *a*-axis-oriented (b) YBCO thin films (300 nm thick) fabricated on different substrates under the identical experimental conditions of 730 °C, 400 mTorr, and 1.2 J/cm^2, which were the conditions for obtaining high crystallinity *c*-axis-oriented YBCO thin films on a $SrTiO_3(100)$ substrate.[14] For obtaining *a*-axis-oriented film, the $PrBa_2Cu_3O_7$ template layer (100 nm thick) was deposited on (100) $SrTiO_3$ substrates at 600 °C prior to YBCO deposition.[17,18] Although the two YBCO films were grown under identical conditions, their surface morphologies were greatly different from each other. A large number of particles were observed on the *c*-axis-oriented film, while much fewer particles were observed in the SEM photograph for the *a*-axis-oriented film. In addition, the *a*-axis-oriented film has a surface smoother than the *c*-axis-oriented film and orthogonally crossing cracks. The crack formation is due to the thermal-expansion mismatch and is discussed in detail elsewhere.[18] If the majority of the particles observed on the *c*-axis-oriented films had originated from the droplets dislodged from the target and impinged to the film surface, similar particles should exist on the *a*-axis-oriented film as well. The droplet origin of particles can also be excluded in our case from the reduced particle formation on the *c*-axis-oriented film deposited on the off-axis $SrTiO_3$ substrate, which will be shown in Sec. III C 2. Combined with these hereafter described results, we can say that the particle originated from droplets can be easily excluded by adjusting PLD conditions and we discuss in this paper the precipitates originated from the phase segregation during the film growth. Here, we call these particles precipitates.

B. Characterization of precipitates

1. Chemical composition of the precipitates

The chemical composition of the precipitates was investigated by AES. Figure 2(a) shows a SEM photograph of a standard high crystallinity YBCO film grown under the conditions described above. The chemical composition of the precipitates is depicted in Figs. 2(b)–2(d) by mapping the intensity of the Auger electron from the film surface. Figures 2(b), 2(c), and 2(d) depict the AES mapping data for Ba, Cu, and Y, respectively. In Fig. 2(d), all the precipitates are shown to have Y deficiency. From Fig. 2(b), the precipitates can be categorized into the two types: deficient in Ba or not. Ba deficient precipitates are rich in Cu compared with the matrix as indicated in Fig. 2(c). From the above results, it is clear that there are two types of precipitates on the film surface: one deficient only in Y and the other deficient both in Y and Ba.

In order to understand the above results, we consulted with the $YO_{1.5}$-BaO-CuO pseudoternary equilibrium phase diagram (Fig. 3) at 850 °C and 1 atm oxygen pressure.[19] According to the literature,[19] the lowest oxygen partial pressure at which the tie lines in the phase diagram are stable is 5.5×10^{-3} atm at 850 °C. Although the film was prepared in a lower oxygen pressure (5.2×10^{-4} atm), we assume the phase diagram is valid for the film-growth process taking the lower substrate temperature (730°C) into account. The compounds which can coexist with YBCO are shown to be

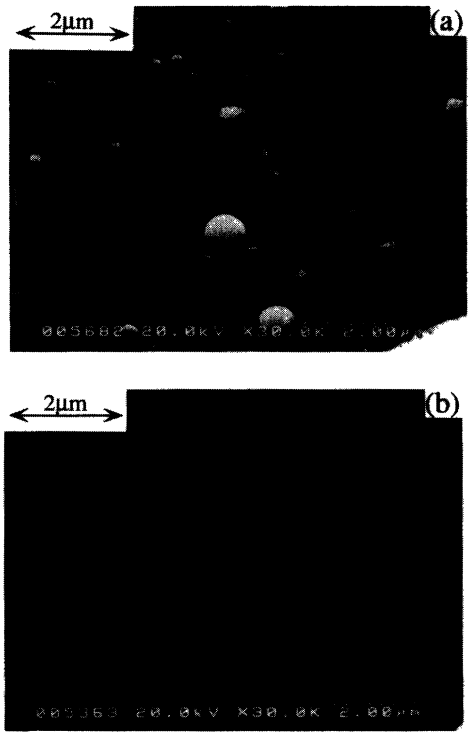

FIG. 1. SEM photographs of high crystallinity YBCO films. (a) *c*-axis-oriented YBCO (300 nm thick) grown on $SrTiO_3(100)$ substrate. (b) *a*-axis-oriented YBCO (300 nm thick) deposited on a PBCO template layer (100 nm thick).

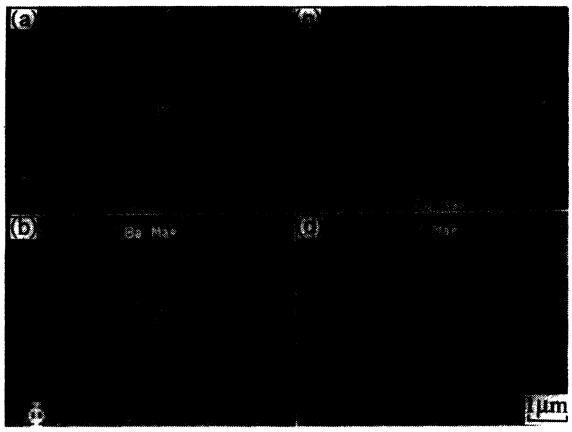

FIG. 2. AES mapping analysis for a surface of high crystallinity *c*-axis-oriented film. (a) SEM image of the analyzed area. (b)–(d) AES mapping images of Ba, Cu, and Y, respectively.

Y_2BaCuO_{5-x}, $BaCuO_2$, and CuO. Among them, Y deficient phases as compared with YBCO are $BaCuO_2$ and CuO, which should appear when the total composition is in the hatched area in the diagram.

In order to quantitatively analyze the composition of the two kinds of precipitates shown in the AES mapping data, point analysis was carried out. As labeled in Fig. 2(a), four points were chosen: numbers 1, 2, and 4 are for three representative precipitates. As a reference, number 3 is selected for the film matrix. The atomic concentrations of Y, Ba, and Cu are listed in column A of Table I. The signal intensities are calibrated with respect to number 3 where the film matrix is assumed to be exact 1-2-3 composition. Although the escaping depth of the Auger electron is only several nm and the incident electron beam diameter is about 30 nm, the penetration depth of the incident electron beam with an accelerating energy of 10 keV is as deep as several μm. As schematically shown in Fig. 4, the electron beam excites Auger electrons not only from the precipitate surface but also from the film surface because of the scattering of incident electrons. Accordingly, the data in column A include not only the signal from the precipitate surface but also the signal

TABLE I. The atomic concentrations of Y, Ba, and Cu for the precipitates (numbers 1, 2, and 4 indicated in Fig. 2) and the matrix film (number 3). Column A: Atomic concentration calibrated by assuming number 3 to be exact Y: Ba: Cu = 1:2:3 composition. Column B: Atomic concentration of precipitates after subtraction of background. Column C: Chemical composition of precipitates corresponding to the data B.

Sampling position	A			B			C
	Y	Ba	Cu	Y	Ba	Cu	
number 1	9.0	41.1	51.5	0	23.0	24.5	$BaCuO_2$
number 2	12.0	39.1	52.1	0	15.0	16.1	$BaCuO_2$
number 3	17.6	35.3	52.9	17.6	35.3	52.9	$YBa_2Cu_3O_{7-\delta}$
number 4	15.7	32.0	67.7	0	0.7	20.8	CuO

from the background film surface. This effect is clearly observed as a pronounced Auger-electron intensity for all three elements at the edge of the precipitates, where the scattered electron beam is more likely to excite Auger electrons from the matrix film surface.

Taking the background signal into account, we recalibrated the data listed in column A of Table I. Assuming that the precipitates contain no Y and the virtual Y signal is attributed to the background from the matrix film, we calculated the atomic concentrations of the precipitates by subtracting the background Y, Ba, and Cu concentrations from the data listed in column A. The values obtained in this way are given in column B, which clearly indicate that the precipitates are $BaCuO_2$ (numbers 1 and 2) and CuO (number 4) as shown in column C. The volume ratio of the precipitate to the matrix film is not more than 10%, if the calculation is made by assuming the precipitate diameter of 1 μm and the density of 10^7 cm^{-2} on a 300-nm-thick film. Such a compositional deviation is smaller than the accuracy of ICP analysis. For instance, ICP analysis showed the total composition of this particular film of Y:Ba:Cu = 1:2.02:2.99. No distinctive deviation from stoichiometry was observed commonly for all the ICP data taken for many of the films discussed in this paper, but it does not necessarily mean

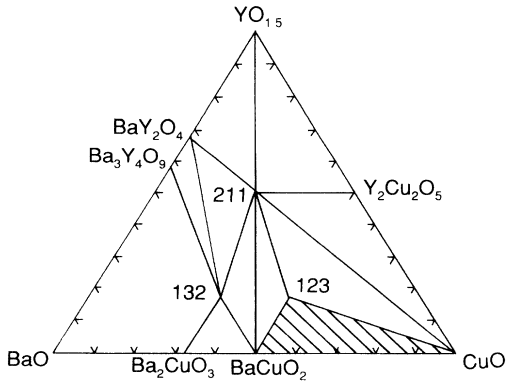

FIG. 3. A pseudoternary phase diagram of $YO_{1.5}$-BaO-CuO at 850 °C and 1 atm of oxygen (Ref. 19).

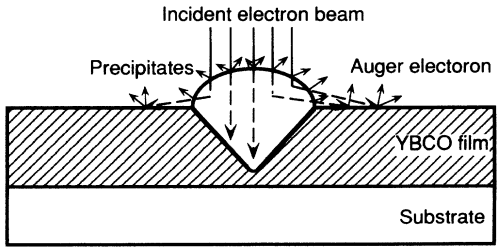

FIG. 4. A schematic view of Auger-electron emission from a precipitate on a film surface. Although the diameter of the incident electron beam is as small as 30 nm and is much smaller than the precipitate diameter, the penetration depth of electron beam is as deep as several μm. Scattering electron beam excites Auger electrons from the background film surface as well. The shape of the precipitate was sketched from the representative cross-section SEM image.

that the composition of species impinging on the film surface during the deposition is exactly stoichiometric. In our case, the total composition of the film should be in the hatched triangle area in Fig. 3, because the three phases existing in the film are YBCO, $BaCuO_2$, and CuO. If we denote the deviation of Ba as x and Cu as y, the film should have a total composition of Y:Ba:Cu=1:2 $+x$:3$+y$, and $y>x$. It is considered that under well-equilibrated and thermally-relaxed conditions, highly crystalline film with almost exact 1-2-3 composition is formed to segregate extra components in secondary phases. If x and y are larger than the solubility limits of BaO and CuO in YBCO, the 1-2-3 phase excludes the other two phases from the bulk film to its surface, thus leading to the formation of a significant amount of precipitates on the film surface.

2. *Relationship between crystallinity and precipitates*

As reported in our previous paper,[14] the film crystallinity was strongly dependent on the growth conditions such as oxygen pressure and laser energy. When the films were prepared under experimental conditions deviated from the optimized conditions in terms of crystallinity, they showed broadened XRD diffraction peaks.

The broadening of XRD peaks in epitaxial YBCO thin film can be evaluated by the full width at half maximum (FWHM) of the Bragg peak as a function of 2θ and it is considered to be related to the local fluctuation in the lattice parameter and lack of lattice coherency along the c axis. Instead of FWHM ($\Delta 2\theta$), we introduce the fluctuation parameter, $\Delta c/c$, which represents the intrinsic fluctuation of the crystal quality along the c axis, in order to quantitatively analyze the crystallinity. The relation between $\Delta c/c$ and $\Delta 2\theta$ can be obtained as the following by differentiating the Bragg formula:

$$\Delta 2\theta=(-2\Delta c/c)\tan(\theta) . \quad (1)$$

Let us first discuss the factors which contribute to the FWHM measurement by using conventional $\theta/2\theta$ XRD. In addition to the fluctuation in the lattice parameter ($\Delta c/c$), two other factors should be taken into account for the observed FWHM. One is the XRD instrumental broadening that can be estimated by measuring FWHM of the Bragg peaks of a Si(111) wafer. The other is the finite film thickness which can be estimated by Sherrer's formula:

$$B=0.9\lambda/t\cos(\theta) , \quad (2)$$

where B is the FWHM, λ is the wavelength of Cu $K\alpha_1$, and t is the film thickness. B increases dramatically when t is less than 50 nm.

The dependences of the above three factors, $\Delta c/c$, instrumental broadening, and B, on Bragg angles are shown in Fig. 5. The solid circles represent the observed FWHM of the (00l) peaks of a YBCO film with the highest crystallinity. The broken lines are the FWHM calculated from Eq. (1) with $\Delta c/c$ of 0.1, 0.15, and 0.2 %. The open rectangles are the measured FWHM of (hhh) peaks of a Si(111) wafer. The dashed line is the FWHM

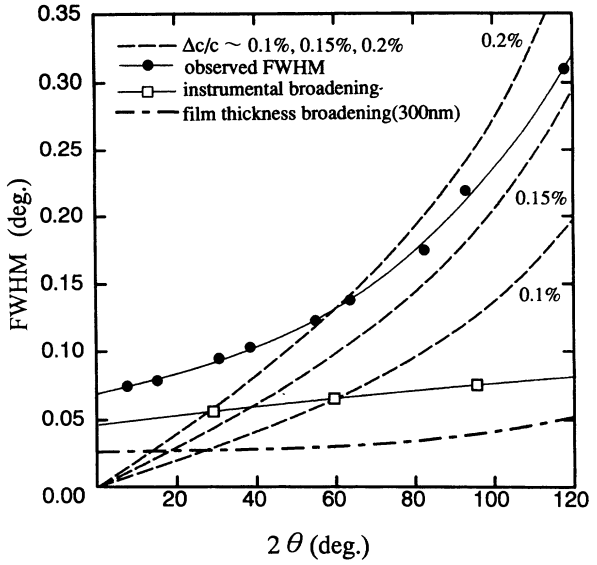

FIG. 5. Dependence of FWHM on Bragg angles. The broken lines are the calculated FWHM from Eq. (1) with $\Delta c/c$ of 0.1, 0.15, and 0.2 %. Solid circles are measured values of (00l) peaks of YBCO film, open rectangles are measured FWHM of (hhh) peaks of Si(111) wafer, and the dashed line is the value estimated from Sherrer's formula (film thickness: 300 nm).

calculated from Sherrer's formula with a film thickness of 300 nm. Figure 5 shows that at low Bragg angles, the FWHM of the XRD peak is dominated by the instrumental broadening and the finite film thickness. With the increase of the Bragg angle, the effect of lattice fluctuation $\Delta c/c$ becomes predominant and the other two effects become negligible. Since it is difficult to deconvolute the observed FWHM into the above three factors, we estimated the lattice fluctuation from $\Delta c/c$ values calculated by Eq. (1) using the FWHM ($\Delta 2\theta$) values measured at high Bragg angles ($>80°$).

The total volume of the precipitates was estimated by assuming that the precipitates have spheric shape. SEM photographs were used for evaluating the size and density of the precipitates. Typically about 100 precipitates were counted at the magnification of 3×10^4 and image size of 8×6 μm^2. Lower magnifications were used for films with lower precipitate densities. Figure 6 shows the relationship between the total volume of the precipitates and the fluctuation parameter ($\Delta c/c$). When the total volume of the precipitates on the film was very large, $\Delta c/c$ was very small, i.e., a high crystallinity of the films. On the contrary, the films with fewer precipitates showed large fluctuations in the c-axis lattice parameter, indicating that there exist a large number of defects in the crystal matrix. Here we should note that the ICP results for the films shown in Fig. 6 revealed no systematic relation with $\Delta c/c$ and the total film composition was almost Y:Ba:Cu=1:2:3 within the experimental error.

Figure 7 shows the dependence of the c-axis lattice parameter on $\Delta c/c$ for about 40 films prepared in this study. The c-axis lattice parameter almost linearly increases with the increase of $\Delta c/c$ for all the films cooled in oxygen atmosphere. Films prepared under the opti-

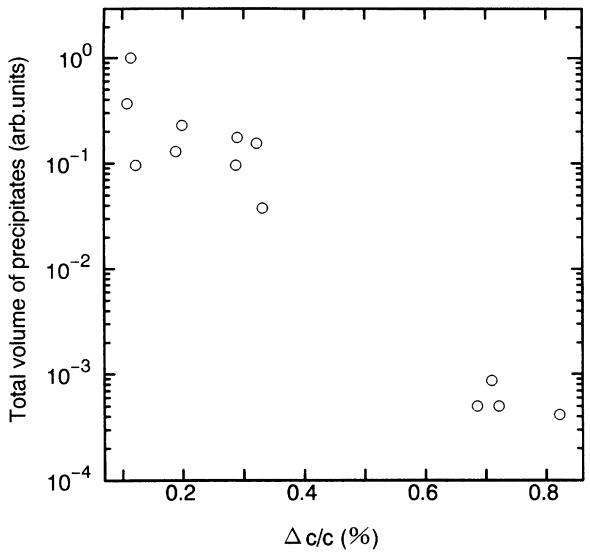

FIG. 6. Relationship between the total volume of the precipitates and the relative fluctuation in c-axis lattice parameter, $\Delta c/c$. The thickness of the film in this figure was about 300 nm.

mized conditions showed $\Delta c/c$ values of 0.1–0.2 % and c-axis lattice parameters of 1.167–1.168 nm. Two of the films that gave values of closed circles in Fig. 7 were made oxygen deficient by annealing in vacuum ($\sim 10^{-8}$ Torr) at 650 °C to give the values marked by closed triangles. Although the oxygen deficiency in the Cu-O chain site of YBCO resulted in the expansion of the

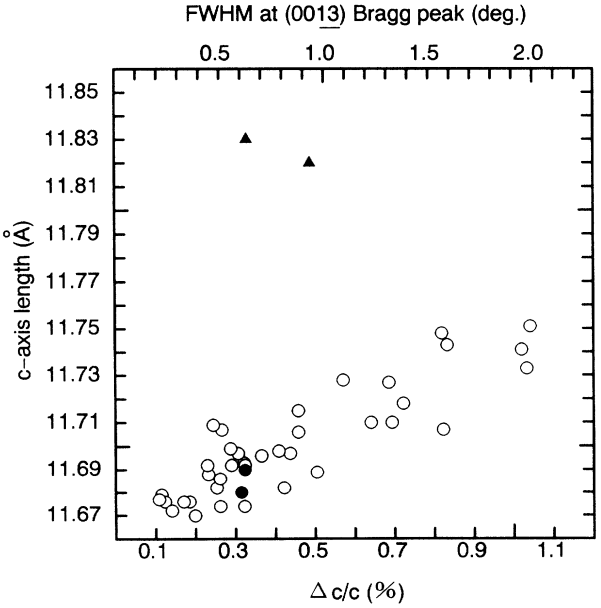

FIG. 7. Relationship between c-axis lattice parameter and the relative fluctuation in c-axis lattice parameter $\Delta c/c$. Open circles represent fully oxidized films cooled in an oxygen atmosphere. Two of these films (closed circles) were vacuum annealed and reanalyzed by XRD. The data for thus prepared oxygen deficient samples were plotted by closed triangles.

c-axis, the fluctuation of the c-axis lattice parameter did not increase significantly.

These results indicate that the expansion and fluctuation in the c-axis parameter have different dependencies; the former depends on both the crystal quality and the oxygen nonstoichiometry, whereas the latter depends on the crystal quality almost exclusively. Thus, the $\Delta c/c$ value is considered to be a better measure of crystal quality than the simple c-lattice parameter. The disorders in the crystal structure that increase $\Delta c/c$ values are presumably introduced due to the kinetic limitation during the film growth where the crystal disorder is quenched in the film.

In a physical vapor deposition process such as PLD, the free energy of the resulting film is essentially identical to that of the starting material (sintered target). The vapor phase precursors evaporated from the target by laser excitation are rapidly cooled at the film surface and incorporated into the crystal matrix through surface migration and chemical reactions. If the reaction and environmental conditions, such as effective oxygen activity and growth step-edge density are appropriate, the surface reaction proceeds within a local thermodynamic equilibrium approximation. In such a case, the crystal matrix is well equilibrated and the free energy of the crystal falls in the energy minimum. If the compositional deviation exceeds the solubility limit of the matrix film, thermodynamically stable phases which can coexist with the matrix film under experimental atmosphere should come out as precipitates. However, if the kinetics dominates the surface reaction process, in such cases of hindered surface migration as at temperature and laser energy lower than the optimum, the system cannot minimize the free energy but is quenched in a metastable local minimum. In such a film, point defects such as Y-Ba antisite, stacking fault, and metastable incoherence of the crystal structure are expected to be frozen. The XRD pattern of these films should become broad and weak compared with that of well-equilibrated films.

The results depicted in Fig. 6 support our hypothesis; when a film was prepared under an optimized condition, the crystal growth proceeds in local thermodynamic equilibrated approximation to form a well-equilibrated and relaxed crystal matrix accompanied by the segregation of off-stoichiometric Ba and Cu into second phases. When the film was prepared under the conditions deviated from the optimized one, the kinetics would become dominant. In this case, the off-stoichiometric Ba and Cu should be incorporated into the film as defects. The incorporation of the impurity phase under this kinetically controlled regime can produce an apparently precipitate-free surface. Previous studies showed that off stoichiometry occluded inside the films caused line and point defects, stacking faults, and precipitates.[4,9,11,13]

So far, we have not mentioned in detail how we changed the crystallinity ($\Delta c/c$) of the films. The process parameters for controlling $\Delta c/c$ included oxygen pressure and laser fluence.[14] The higher the oxygen pressure, the higher the crystallinity. There was optimum laser fluence (1.1–1.2 J/cm^2) to get high crystallinity film, keeping the oxygen pressure at 400 mTorr. The

lower fluence degraded the film crystallinity and the higher fluence resulted in inhomogeneous film probably because the film surface was exposed too much to the plume. We speculate that the effective oxygen activity dominated by the plasma plume plays an important role in determining the competition between the thermodynamics and kinetics of the crystal-growth process; higher oxygen activity is essential in enhancing the surface migration and surface reaction by which the system is facilitated to reach local thermal equilibrium. At a constant substrate temperature, the shape and color of the plume changed depending on oxygen pressure and laser energy density adjusted by the lens focus. Empirically, high crystallinity films can only be obtained when the laser plume is reddish and with the plume head almost touching the growing film surface. For example, with the increase of oxygen pressure from 100 mTorr to 400 mTorr, the plume changed from greenish to reddish and enhanced film crystallinity resulted.[14] The optical emission spectroscopy showed that both elemental and oxide species ejected from the target increased their emission intensities with the increase of oxygen pressure, and that the oxide emission had a stronger pressure dependence than the elemental emission.[20]

C. Nucleation and growth of precipitates

1. *Film thickness dependence of precipitates*

In order to clarify the mechanism of the precipitate formation, the film thickness dependence of precipitate density and size was investigated. The films investigated here were prepared under the optimized conditions in terms of crystallinity. The size distribution of precipitates for the three samples with different film thicknesses (50, 200, and 300 nm) was analyzed. The precipitate density was calculated by counting the number of precipitates larger than 50 nm. Five SEM photographs (magnification of 3×10^4, image area of 8×6 μm^2) were used for every sample. The 50-nm-thick film had 2×10^8 cm^{-2} precipitates of about 50–100 nm in diameter. The thicker (200 and 300 nm) films had the same density in total number of precipitates but their size distribution ranged wider from 50 to 800 nm. The fact that no distinct increase in the total precipitate density was observed for the thicker films indicates that the nucleation of precipitates occurs during the initial 50-nm film growth. The cross-sectional SEM observation revealed that the precipitates grew in such a way as shown in Fig. 4. This result reinforced the increase of precipitate size with the increase of film thickness.

2. *Effect of substrate misorientation*

In Sec. III B 2, we proposed the concept of competition between thermodynamics and kinetics; the precipitate formation takes place when thermodynamics rather than kinetics dominates the surface process. Then we expected that the competition between thermodynamics and kinetics could be controlled by using a misorientated substrate. The crystal-growth mode should be affected by the substrate morphology (step density) at the initial film-growth stage.

Three sets of experimental conditions, *A*, *B*, and *C*, were chosen to investigate the misoriented (tilted) substrate effect.

A: optimized condition in terms of crystallinity with focused laser fluence, corresponding to $\Delta c/c<0.2\%$ in Fig. 6;

B: slightly defocused laser fluence, corresponding to $0.2\%<\Delta c/c<0.5\%$;

C: totally defocused laser fluence, corresponding to $\Delta c/c>0.5\%$. Exact substrates were also used for comparison.

For the films prepared under the intermediate conditions (*B*), the misorientation of the substrate surface gave a dramatic decrease in precipitate density. The density of precipitates which were visible by SEM (>50 nm) was suppressed by three orders of magnitude for the film grown on a misoriented substrate ($\sim10^5/cm^2$) as compared with the film grown on an exact substrate ($\sim10^8/cm^2$). The crystallinity of the film grown on a misoriented substrate was poorer ($\Delta c/c\sim0.5\%$) than that grown simultaneously on an exact substrate ($\Delta c/c\sim0.3\%$). Such a misoriented substrate effect, however, was not so clear when films were prepared under two extreme conditions of high crystallinity (*A*) and poor crystallinity (*C*).

D. A possible mechanism of precipitate formation

Under the deposition conditions we employed, the nucleation of the precipitates occurred at the initial stage of film growth apparently due to the supersaturation of impurity phases. Acting as impurity gettering centers, the nuclei once formed can prevent the local supersaturation of the impurity phase and suppress further nucleation of precipitates. Thus, the precipitate density of about $10^8/cm^2$ is kept constant. Since the precipitate density is much lower than the screw dislocation density ($10^9/cm^2$), the migration distance of excess species should be as long as several μm, far longer than the terrace widths of the spirals. This indicates that the impurity species can migrate across steps to reach the gettering centers. Since the flux of extra components to be incorporated into a precipitate should be proportional to its interface area with the matrix film, larger precipitates would grow faster than smaller ones to give an inhomogeneous distribution in precipitate size. This should be the situation occurring under the optimized growth condition, i.e., the thermoequilibrated state to form films with $\Delta c/c$ smaller than 0.2%. When the film preparation conditions gradually deviated from the optimized one, the crystal-growth process would become dominated kinetically to form films with $\Delta c/c$ values higher than 0.5%. In this case, extra components adsorbed on the surface would be incorporated into the crystal before they could diffuse to a gettering center.

Cross-sectional TEM, STM, and atomic force microscope observations revealed that the *c*-axis-oriented YBCO grew in a layer-by-layer manner along the film surface by incorporating species impinging from the gas

phase at step edges.[21–25] As far as this step-edge growth mode is concerned, the growth mode should be sensitive to the step density. At the initial stage of growth on an exact substrate, the terrace width is much larger than the surface diffusion length. This large terrace width leads to the supersaturation of off-stoichiometric elements and thus results in two-dimensional nucleation of both the 1-2-3 phase and the segration phase. A misoriented substrate provides a large number of step edges which would facilitate the crystal growth, since the migrating precursors can find step edges to be incorporated in the crystal, the supersaturation at the initial stage of film growth would be suppressed.

The above discussion is consistent with the observation that the *a*-axis-oriented films showed much fewer precipitates. The charge neutral unit lattice along the *a* axis is composed of two atomic layers, which is much less than six atomic layers along the *c* axis. Moreover, all atomic planes (Y, BaO, CuO, CuO_2) expose their edges to the film surface. These factors are expected to facilitate the kinetically dominated crystal growth. In such a case precipitates would not be formed so much.

As the origin of the precipitate nuclei, droplets which are too small to be detected and dislodged from the target and impinged to the film surface are also plausible. Some geometric arrangements such as off-axis deposition[1] and the crossed fluxes technique[16] were reported to be effective to reduce this kind of particle. In our case, precipitates of this origin can be excluded as shown by this misorientated substrate effect.

IV. CONCLUSIONS

The formation of surface precipitates of YBCO epitaxial films grown by pulsed laser deposition was analyzed from various viewpoints. Two kinds of precipitates, $BaCuO_2$ and CuO, existed on the film surface as clarified by AES. A well-equilibrated and relaxed crystal matrix excludes the off-stoichiometric part (several percents) to the film surface as precipitates. Incorporation of the off stoichiometry into the film matrix results in the formation of a nonequilibrium solid solution with large amount of defects in the film which displays expansion and fluctuation in the *c*-axis lattice parameter. By changing the film fabrication condition, the crystallinity and the surface precipitate density can be controlled. It would be necessary for us to obtain a film with an excellent crystallinity (superconductivity) precipitate-free surface, so that the film composition is exactly controlled to the stoichiometric ratio by using an *in situ* composition monitoring system at the growing film surface.

ACKNOWLEDGMENTS

We thank T. Morohashi at ULVAC-PHI, Inc. for the AES measurement. This work was supported in part by a Grant-in-Aid for Scientific Research from the Ministry of Education, Science and Culture, NEDO under the management of R&D of Basic Technology for Future Industries, and Iketani Science Foundation.

---

*Present address: Division of Biological Sciences, Graduate School of Science, Hokkaido University, Sapporo 060, Japan.
†Author to whom correspondence should be addressed.

[1] B. Holzapfel, B. Roas, L. Schultz, P. Bauer, and G. Saemann-Ischenko, Appl. Phys. Lett. **61**, 3178 (1992).
[2] R. K. Singh, D. Bhattacharya, and J. Naraya, Appl. Phys. Lett. **61**, 483 (1992).
[3] B. Wuyts, Z. X. Gao, S. Libbrecht, M. Maenhoudt, E. Osquiguil, and Y. Bruynseraede, Physica C **203**, 235 (1992).
[4] T. I. Selinder, U. Helmersson, Z. Han, J. E. Sundgren, H. Sjostrom, and L. R. Wallenberg, Physica C **202**, 69 (1992).
[5] Y. Q. Li, J. Zhao, C. S. Chern, P. Lu, B. Gallois, P. Norris, B. Kear, and F. Cosandey, Physica C **195**, 161 (1992).
[6] J. A. Edwards, N. G. Chew, S. W. Goodyear, S. E. Blenkinshop, and R. G. Humphries, J. Less-Common Met. **164**, 414 (1990).
[7] J. Zhao, C. S. Chern, Y. Q. Li, P. Norris, B. Gallois, B. Kear, X. D. Wu, and R. E. Munchausen, Appl. Phys. Lett. **58**, 2839 (1991).
[8] C. C. Chang, X. D. Wu, R. Ramesh, X. X. Xi, T. S. Ravi, T. Venkatesan, D. M. Hwang, R. E. Munchausen, S. Foltyn, and N. S. Nogar, Appl. Phys. Lett. **57**, 1814 (1990).
[9] O. Eibl and B. Roas, J. Mater. Res. **5**, 2620 (1990).
[10] M. J. Casanove, A. Alimoussa, C. Roucau, C. Escribe-Filippini, P. L. Reydet, and P. Marcus, Physica C **175**, 285 (1991).
[11] A. Catana, R. F. Broom, J. G. Bednorz, J. Mannhart, and D. G. Schlom, Appl. Phys. Lett. **60**, 1016 (1992).
[12] A. Catana, J. G. Bednorz, Ch. Gerber, J. Mannhart, and D. G. Schlom, Appl. Phys. Lett. **63**, 553 (1993).
[13] A. F. Marshall, V. Matijasevic, P. Roesenthal, K. Shinohara, R. H. Hammond, and M. R. Beasley, Appl. Phys. Lett. **57**, 1158 (1990).
[14] M. Kawasaki, J. P. Gong, M. Nantoh, T. Hasegawa, K. Kitazawa, M. Kumagai, K. Hirai, K. Horiguchi, M. Yoshimoto, and H. Koinuma, Jpn. J. Appl. Phys. **32**, 1612 (1993).
[15] The high crystallinity films show T_c (zero) of 91 K, ΔT_c (10–90 %) of less than 1 K and J_c at 77 K of greater than 2×10^6 Å/cm^2. The detailed results were reported in Ref. 14.
[16] M. D. Strikovsky, E. B. Klyuenkov, S. V. Gaponov, J. Schubert, and C. A. Copetti, Appl. Phys. Lett. **63**, 1146 (1993).
[17] A. Inam, C. T. Rogers, R. Ramesh, K. Remschnig, L. Farrow, D. Hart, T. Venkatesan, and B. Wilkens, Appl. Phys. Lett. **57**, 2484 (1990).
[18] K. Fujito, M. Kawasaki, J. P. Gong, R. Tsuchiya, M. Yoshimoto, and H. Koinuma (unpublished).
[19] B. T. Ahn, V. Y. Lee, R. Beyers, T. M. Gur, and R. A. Huggins, Physica C **167**, 529 (1990).
[20] X. D. Wu, B. Dutta, M. S. Hegde, A. Inam, T. Venkatesan, E. W. Chase, C. C. Chang, and R. Howard, Appl. Phys. Lett. **54**, 179 (1989).
[21] T. Terashima, Y. Bando, K. Iijima, K. Yamamoto, K. Hirata,

K. Hayashi, K. Kamigaki, and H. Terauchi, Phys. Rev. Lett. **65**, 2684 (1990).

[22]S. K. Streiffer, B. M. Lairson, C. B. Eom, B. M. Clemens, J. C. Bravman, and T. H. Geballe, Phys. Rev. B **43**, 13 007 (1991).

[23]S. J. Pennycook, M. F. Chisholm, D. E. Jesson, R. Fenstra, S. Zhu, X. Y. Zheng, and D. J. Lowndes, Physica C **202**, 1 (1992).

[24]M. Hawley, I. D. Raistrick, J. G. Beery, and R. J. Houlton, Science **251**, 2587 (1991).

[25]C. Gerber, D. Anselmetti, J. G. Bednorz, J. Mannhart, and D. G. Schlom, Nature (London) **350**, 279 (1991).

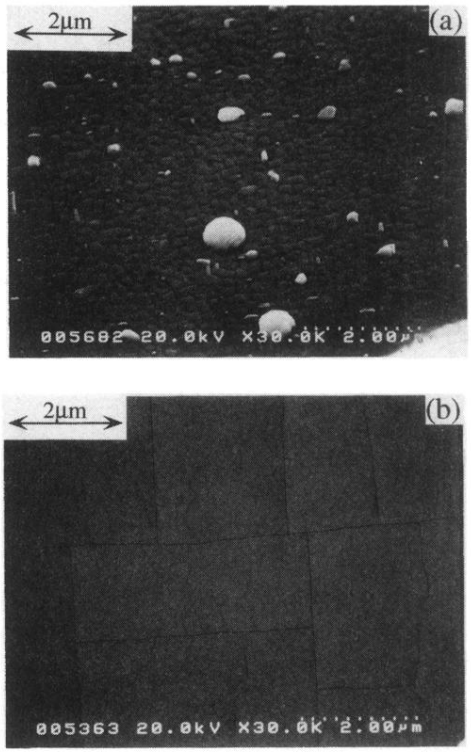

FIG. 1. SEM photographs of high crystallinity YBCO films. (a) *c*-axis-oriented YBCO (300 nm thick) grown on $SrTiO_3(100)$ substrate. (b) *a*-axis-oriented YBCO (300 nm thick) deposited on a PBCO template layer (100 nm thick).

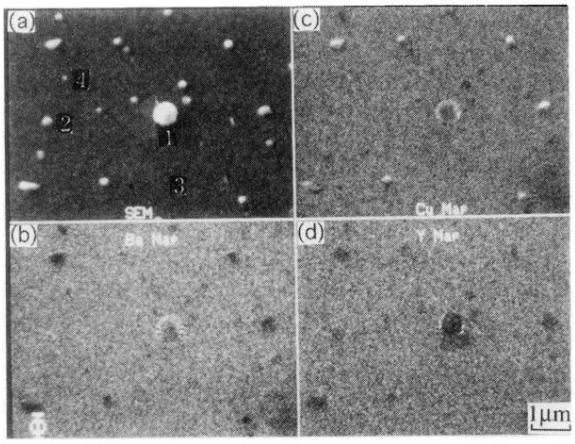

FIG. 2. AES mapping analysis for a surface of high crystallinity *c*-axis-oriented film. (a) SEM image of the analyzed area. (b)–(d) AES mapping images of Ba, Cu, and Y, respectively.